Journal of Materials Chemistry C

PAPER

View Article Online
View Journal | View Issue

Cite this: J. Mater. Chem. C, 2015, 3, 3629

Highly transparent and flexible polyimide–AgNW hybrid electrodes with excellent thermal stability for electrochromic applications and defogging devices†

Heng-Yi Lu,‡ Chin-Yen Chou,‡ Jia-Hao Wu, Jiang-Jen Lin and Guey-Sheng Liou*

Received 15th January 2015,
Accepted 25th February 2015

DOI: 10.1039/c5tc00142k

www.rsc.org/MaterialsC

In this study, highly transparent and flexible electrodes with the highest thermal stability were successfully prepared from silver nanowire (AgNW)–polyimide (PI) hybrid solutions by facile solution casting on insoluble polyimide substrates without any troublesome transferring process. The prepared highly flexible AgNW–PI electrodes exhibit a low resistance of 25 Ω sq^{-1} and high transmittance up to 86% at a wavelength of 550 nm. Thus, by introducing high performance polyimide as a binder, the obtained colorless AgNW electrodes show improved adhesion properties between the AgNWs and the substrates as well as excellent thermal stabilities and high glass transition temperatures (T_g) above 300 °C. Furthermore, the resulting AgNW–PI hybrid colorless electrodes could maintain the conductivity even after folding more than 1000 times. Thus, these optically transparent AgNW–PI hybrid electrodes have extremely high potential to operate at high temperatures in the working environment or post processing.

1. Introduction

With advances in technology, a variety of new components for computers, communication devices and consumer electronics have sprung up over the last two decades. Advances in materials are essential to enhance the properties of both high conductivity and transmittance. This important research topic has attracted great attention by investigating carbon nanotubes (CNTs),[1] graphene,[2] metal oxides, and metallic nanowires.[3,4] Though indium tin oxide (ITO) has excellent properties in both electronics and optics, there are some serious problems with this compounds, such as the high cost of indium and the brittle properties of ITO. Thus, some strategies have been adopted to obtain new hybrid materials for preparing flexible and transparent electrodes. For example, CNTs have been studied since 1991, and the electrodes made with CNTs show a sheet resistance of 200 Ω sq^{-1} and a transmittance of 80% at 550 nm.[5] However, this performance is still not good enough for the commercial requirements. Another member of the carbon family, graphene, has also attracted a great deal of attention since the discovery of graphene was awarded the Nobel Prize in Physics in 2010. Nevertheless, single layer and few layer graphene that satisfy the requirements of transparent conductive electrodes can only be prepared by the chemical vapor deposition method (CVD). However the CVD method requires very high temperatures and vacuum degrees, and the additional process of transferring is necessary for CVD graphene. Therefore, silver nanowires (AgNWs) have been considered as the most potential candidate to replace ITO in the future.[3] The most widely used method for generating AgNWs is template-directed synthesis.[6] However, this method has problems such as producing an irregular morphology, low aspect ratio, and low yield. In 2002, Xia's group first proposed a polyol process to produce AgNWs as a simple and large scale method,[7] which used poly(vinylpyrrolidone) (PVP) as a capping agent and ethylene glycol (EG) as a reductant to reduce the silver nitrate. In order to obtain transparent electrodes from AgNWs, many attempts, such as preparation, coating methods and annealing of AgNWs, have been reported.[8–21] Some applications of transparent conductive electrodes obtained from AgNWs have been reported, such as solar cells,[22–27] touch screens,[28] heaters,[29–33] and light-emitting diodes.[21,34–36] In addition, the transparent electrodes derived from AgNWs also have potential to be applied as transparent electrochromic devices (ECD) and memory devices.[37–39]

For practical applications, the poor adhesion properties of AgNWs and the lower T_g of flexible substrates are crucial issues related to AgNW–polymer hybrid electrodes. Therefore, some approaches have been used to improve these problems, such as using polyethylene oxide as the polymer binder,[40] or using conducting polymer poly(3,4-ethylenedioxythiophene):poly(styrene-sulfo-nate) (PEDOT:PSS), heat-resistant copolymers or colorless

Functional Polymeric Materials Laboratory, Institute of Polymer Science and Engineering, National Taiwan University, 1 Roosevelt Road, 4th Sec., Taipei 10617, Taiwan. E-mail: gsliou@ntu.edu.tw

† Electronic supplementary information (ESI) available: Basic properties of the synthesized polyimides. See DOI: 10.1039/c5tc00142k

‡ Equal contribution to this work.

polyimide as protectors.[30,33,41,42] However, the complex synthesis procedures, organic-soluble behavior, and deep coloration of these polymers were insufficient to endure high temperatures or post film-processing for practical applications.

In this study, thermally stable and colorless polyimide (PI) with a high T_g and high transmittance in the visible light region was chosen as a binder to prevent the AgNWs from peeling off. To the best of our knowledge, this is the first time AgNW–PI hybrid electrodes have been prepared with not only low electrical resistance, excellent optical transparency, and flexibility, but also a high thermal stability that could withstand the high temperature during the annealing process or when working as a heater. Furthermore, the multifunctional applications of AgNW–PI electrodes have also been developed by the combination of an electrochromic polymer. Because of the adoption of polyimide substrates and electrochromic materials, smart windows with defog or desnow functions would have great potential for practical applications in the future.

2. Experimental

2.1 Materials

Silver nitrate (99.85%, ACROS), polyvinylpyrrolidone (PVP) (M_w = 58 000, ACROS), ethylene glycol (EG) (SHOWA), copper(II) chloride (98%, SHOWA), lithium tetrafluoroborate (98%, ACROS), heptyl viologen (TCI), *N*-methyl-2-pyrrolidinone (NMP) (TEDIA), *N,N*-dimethylacetamide (DMAc) (TEDIA), acetic acid glacial (SCHARLAU), pyridine (TEDIA), acetic anhydride (>99%, Sigma-Aldrich), and poly-L-lysine solution (0.1 wt%, Ted Pella) were purchased and used without purification. Commercially available monomers, 3,3′,4,4′-biphenyltetracarboxylic dianhydride (BPDA) (Chriskev), 2,2-bis(3,4-dicarboxyphenyl)hexafluoropropane dianhydride (6FDA) (Chriskev), and 4,4′-(hexafluoroiso-propylidene)dianiline (98%, ACROS), were purified by sublimation. *trans*-1,4-Cyclohexanediamine (99%, ACROS) was purchased and purified by recrystallization from *n*-hexane to get white crystals. 2,2′-Bis(trifluoromethyl)-benzidine (TFMB), 1,2,4,5-cyclohexane tetracarboxylic dianhydride, and PMMA (M_w: 120 000) were supplied by the Industrial Technology Research Institute of Taiwan. TFMB was purified by recrystallization from ethanol and water to get white crystals, while 1,2,4,5-cyclohexane tetracarboxylic dianhydride was dried in a vacuum oven at 120 °C for 6 hours. Electrochromic polyamide triphenylamine-containing polyamide (TPA–PA) was synthesized according to previously reported procedures.[43]

2.2 Synthesis of colorless polyimides

The colorless polyimide 6FCHPI and copolymer used in this study were synthesized according to a conventional two-step method by chemical and thermal imidization, consecutively, as shown in Scheme 1.[44,45] The PI binder 6FCHPI was synthesized as follows: 0.2442 g (1 mmol) of 1,2,4,5-cyclohexane tetracarboxylic dianhydride was added in one portion (30 wt% solid content) into a solution of 0.3343 g (1 mmol) of diamine 4,4′-(hexafluoroiso-propylidene)dianiline in 1.4 mL of DMAc at room temperature under a nitrogen flow. The mixture was stirred at room temperature

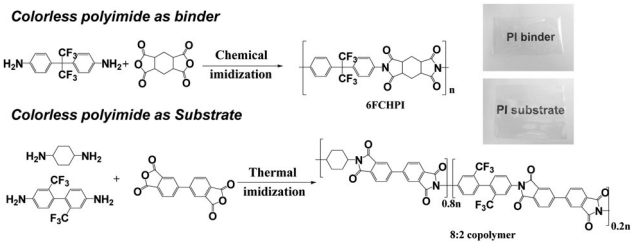

Scheme 1 The synthetic scheme for the synthesis of colorless polyimide 6FCHPI and 8 : 2 copolymer.

for about 3 days. Then, pyridine (0.4 mL) and acetic anhydride (0.95 mL) were added into the reactor, and the imidization reaction proceeded at room temperature over 12 h. The resulting polymer solution was poured into 200 mL of methanol giving a white precipitate, which was collected by filtration.

The PI substrate was synthesized as follows: 0.1827 g (1.6 mmol) of *trans*-1,4-cyclohexanediamine was dissolved in DMAc at 70 °C under a nitrogen flow, and cooled down to room temperature. Then, 0.2112 g (3.52 mmol) of acetic acid was added slowly to form the salt. Subsequently, 0.5884 g (2 mmol) of BPDA was added into the solution. After mechanical stirring for 3 hours at room temperature, another diamine (0.1281 g, 0.4 mmol) of TFMB was added to react for another 3 hours. The obtained PAA solution was coating on a glass substrate to form a PI thin film. Finally it was dried *in vacuo* at room temperature overnight, then the temperature was raised slowly to 300 °C for 1.5 hours to complete the thermal imidization.

2.3 Synthesis of silver nanowires

AgNWs were prepared by the modified polyol process: ethylene glycol (50 mL) was added into a 250 mL three necked flask, and stirred at 155 °C for one hour under a nitrogen flow. At the same time, separate solutions of silver nitrate (0.094 M) and PVP (0.147 M) in 15 mL of ethylene glycol were prepared. After preheating for an hour, 400 μL of 4 mM copper(II) chloride in EG was added into the reactor and stirred for 15 minutes. The PVP solution was then added in one go and the $AgNO_3$ solution was added drop by drop. Finally, the resulting AgNWs were obtained after another one hour reaction, then washed by ethanol with centrifugation filtration many times to remove the residual PVP and silver nanoparticles.

2.4 Fabrication of AgNW–PI electrodes

The schematic diagram of the fabrication procedure for the AgNW–PI electrodes is depicted in Fig. 2a. By using a solvent exchange method, the AgNWs were firstly transferred from ethanol to DMAc, and the weight fraction of the AgNWs in the DMAc solution was measured by thermogravimetry analysis. Then, the PI solutions with various concentration of AgNWs (80–320 mg m^{-2}) were coated on the substrates, which were immersed in poly-L-lysine water solution for a while.[46] After drying *in vacuo* to form the random network of AgNWs, thermal annealing at 180 °C for an hour was carried out to decrease the electrical resistance of the AgNW–PI hybrid electrodes.

The thickness of the dried film was about 10 μm, as observed by optical microscopy, shown in Fig. S2 (ESI†).

2.5 Fabrication of the electrochromic device using AgNW–PI hybrid electrodes

The fabrication of the electrochromic device (ECD) shown in Fig. 6a, and the electrochromic polymer films were prepared by spinning a solution of TPA–PA (50 mg mL^{-1} in DMAc) onto an ITO-coated glass substrate (25 × 25 × 0.7 mm, 5–10 Ω sq^{-1}). The spin-coated polymer was dried on a hotplate and the edge of the polymer was removed to obtain a sample with a final active area of about 20 × 20 mm^2. A gel electrolyte based on PMMA (1.25 g) and $LiBF_4$ (0.15 g) was plasticized with propylene carbonate (2.75 g) to form a highly transparent and conductive gel. In addition, heptyl viologen ($HV(BF_4)_2$) (0.03 g) was added as a counter electrode species or ion storage layer. The gel electrolyte was spread on the polymer-coated side of the electrode, and the AgNWs–PI was then covered onto the electrolyte layer as a top electrode.

2.6 Characterization of the AgNW–PI electrodes

Thermogravimetric analysis (TGA) with a TA instrument Q50 was used to measure the thermal stability of the polymers and hybrids. Field emission scanning electron microscopy (FE-SEM, JEOL, JSM-6700F), transmission electron microscopy (TEM, JEOL JEM-1230), and optical microscopy (HRM-300) were used to examine the surface morphology and microstructure of the AgNWs and hybrid films. UV-vis spectra of the polymers and hybrid films were recorded using a Hitachi U-4100 UV-vis-NIR spectrophotometer in the wavelength range of 300–800 nm. The resistance and sheet resistance of the transparent electrodes were measured using a handheld LCR meter (Agilent U1732C) and four point probes (Keithlink Technology), respectively. An electrical thermometer (TES 1310 TKPE-K) was used to measure the temperature of the defrost device.

3. Results and discussion

3.1 Basic characterization

The substrate materials used in this study are shown and characterized in Scheme 1, and Tables S1 and S2 (ESI†). All polymerization reactions proceeded homogeneously and gave high molecular weights that could afford tough, flexible, and transparent films *via* solution coating. Furthermore, the PI binder exhibited good solubility in common organic solvents, such as DMAc and NMP, which provided an easy blending method with AgNWs. On the other hand, the PI substrate showed excellent chemical resistance to these common organic solvents.

The optical properties are tabulated in Table S3 (ESI†). The transmittance at 450 nm of these two PIs was higher than 80% with a cutoff wavelength lower than 400 nm. By a proper structural design, the charge transfer effect could be depressed to result in a colorless polyimide. The introduction of high electronegative bulky fluorine atoms or adopting aliphatic monomers could decrease the charge transfer effect. Therefore, transparent, colorless, and soluble polyimide could be prepared from aliphatic dianhydride and fluorine-containing diamine by chemical imidization, while the PI substrate with a high chemical resistance was obtained by thermal imidizaiton from fluorine-containing and aliphatic diamine monomers with aromatic dianhydride BPDA. These prepared polyimides have excellent thermal stabilities, and the diagrams of the thermogravimetric and thermomechanical analyses of the PIs are depicted in Fig. 1a and b, respectively, and the results are summarized in Table S4 (ESI†). The T_g values of these two PIs were higher than 325 °C, and 5 wt% decomposition temperatures were also higher than 450 °C even in air, indicating that the PIs are highly thermally stable. Moreover, the coefficient of the thermal expansion of the PI substrate was only 8 ppm per °C, which means it could maintain the dimensions and endure large temperature variations in the environment.

3.2 Properties of the AgNW–PI hybrid based transparent electrode

The scheme of the procedure and the transparency of the AgNWs and AgNW–PI hybrids are shown in Fig. 2. The AgNWs were prepared by a modified polyol process that used EG as the reductant and solvent, PVP as the capping agent, silver nitrate as the provider of silver cations, and copper chloride as the oxygen scavenger. The obtained AgNWs have an average diameter around 100 nm and an average length of 35 μm. The morphology of the AgNWs was measured by SEM and TEM, and these images are depicted in Fig. 2b and c. The average aspect ratio of these AgNWs was around 350, which is high enough for transparent electrodes.

By using this facile approach, hybrid electrode films with high transmittance and low sheet resistance could be readily prepared. UV-vis spectra of the obtained electrodes with different amounts of AgNWs on the glass are summarized in Fig. 2d. In the case of only 80 mg m^{-2} AgNWs, the transmittance at 550 nm was up to 93%, but the sheet resistance was too high to be an electrode. Therefore, by increasing the amount of AgNWs to 200 mg m^{-2}, the transmittance of electrode was higher than 80% at 550 nm with a sheet resistance of only 11 Ω sq^{-1}, which is comparable to the commercial ITO electrodes. Fig. 2e exhibits the amount of AgNWs plotted against the sheet resistance of the AgNW–PI hybrid electrodes. It is very difficult to achieve a high transmittance and low resistance simultaneously due to the dilemma relationship between transmittance and conductivity. The figure of merit (FoM) is a quantity used to characterize the

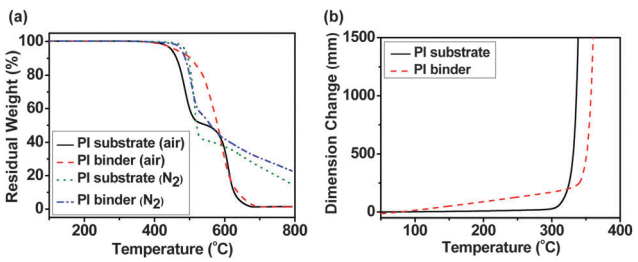

Fig. 1 (a) Thermogravimetric analysis of the polyimides at a scan rate of 20 °C min^{-1}. (b) Thermomechanical analysis curves of the polyimides.

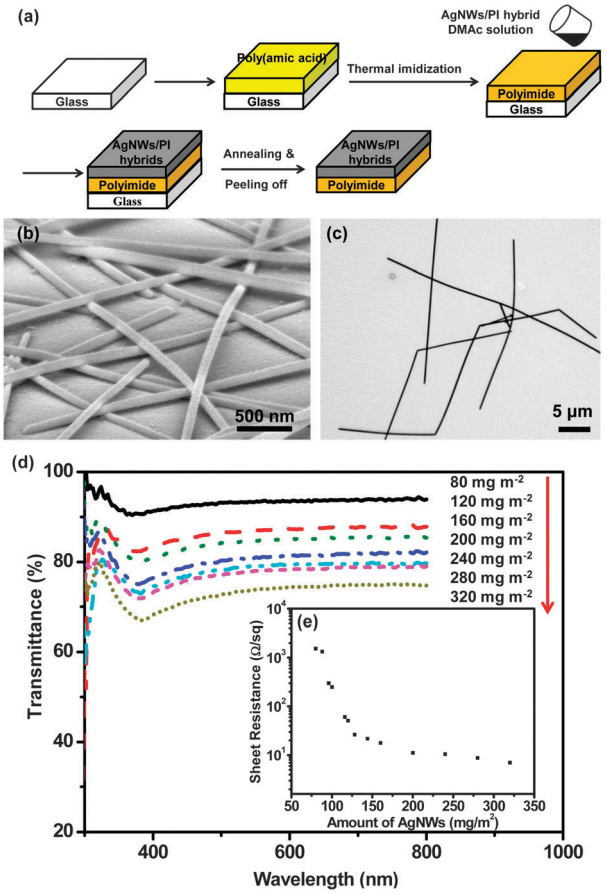

Fig. 2 (a) The scheme of the procedure for the transparent AgNW–PI hybrid electrodes. Two kinds of PI were used as both the binder and substrate. (b) SEM image of the AgNWs tilted at 60 degrees. (c) TEM image of the AgNWs. (d) UV-vis transmittance spectra of the resulting electrodes with various amounts of AgNWs coated on the glass (the transmittance is based on the glass substrate as the reference). (e) Amount of AgNWs plotted against the sheet resistance values of the AgNW–PI hybrid coated on glass.

performance of transparent conductors,[47–49] and the FoM for transparent electrodes can be expressed by:

$$\frac{\sigma_{dc}}{\sigma_{op}(\lambda)} = \frac{Z_0}{2R_s}\frac{\sqrt{T}}{1-\sqrt{T}} \quad (1)$$

where σ_{dc} is the DC conductivity of the film, $\sigma_{op}(\lambda)$ is the optical conductivity at a wavelength of λ nm, Z_0 is the impedance of free space (377 Ω), R_s is the sheet resistance, and T is the transmittance at λ nm. For industrial applications, the FoM values should be larger than 35.[50] The FoM values of the AgNW–PI hybrid electrodes in this study could reach 160, implying that the transparent electrodes fabricated by this facile approach have an excellent combination of good optical and electrical properties.

Furthermore, AgNWs coated on PI substrates were also investigated, and a highly flexible PI electrode with a low resistance of 25 Ω sq^{-1} and a high transmittance of about 86% could be obtained successfully. For comparison, the folding test of the commercial ITO coated polyethylene naphthalate (PEN) electrode shown in Fig. 3a was used as a reference. The ITO–PEN electrode

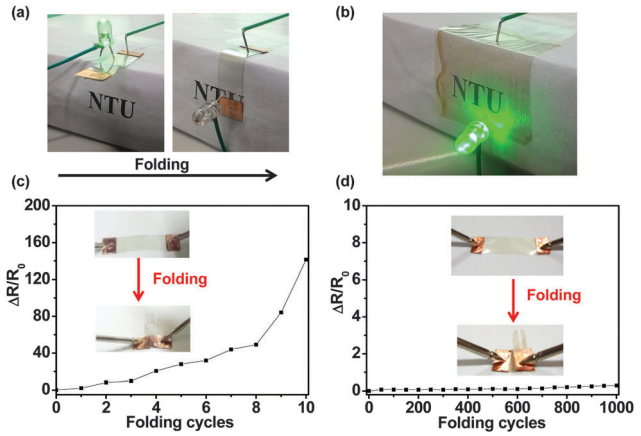

Fig. 3 (a) The ITO coated PEN lost conductivity immediately after folding, thus the LED lamps no longer worked. (b) The AgNW–PI hybrid electrode connected to a LED array. The LED lamps kept working even under continuous folding conditions. (c) The change in resistance after folding for the ITO coated PEN electrodes. The *Y*-axis represents the change in resistance divided by the original resistance. (d) The change of resistance after 1000 folding cycles for the AgNW–PI hybrid electrodes.

connected to LED lamps lost conductivity very quickly while folding, and the lamps no longer worked. Nevertheless, the AgNW–PI electrodes kept the lamps working well even on folding because the good ductility of the nanowire networks could prevent breaking down under folding (Fig. 3b). In addition, the resistance change with folding cycles for these two different electrodes were compared. The resistance change of ITO–PEN increased to 140 times that of the pristine material after only 10 cycles of folding as shown in Fig. 3c, while the AgNW–PI electrode exhibited excellent flexibility, revealing almost no change in resistance even after 1000 folding cycles (Fig. 3d).

Although the AgNW electrodes are equipped with good conductivity, flexibility, and high transmittance, the adhesion between the AgNWs and the substrate is too weak for long-term applications. Introducing colorless polyimide into the nanowires not only binds the AgNWs tightly to the substrates but also promotes the dispersion of the AgNWs. The peeling off test was used to evaluate the behavior by using 3 M scotch tape. The pristine AgNWs are easily removed from the substrates as shown in Fig. 4a, while the AgNWs with the polyimide binder showed extremely strong adhesion to the substrates (Fig. 4b). Moreover, the AgNWs–PI hybrid showed thermal stability at temperatures higher than 200 °C, attributed to the highly thermal stability of PI substrate.

3.3 Properties of the AgNW–PI heater (defogging device)

The defogging device fabricated by the hybrid electrodes could remove water effectively within one minute when a potential of 6 V was applied (Fig. 5a) due to the excellent performance of producing thermal energy according to Joule's law described as follows:

$$Q = \frac{V^2}{R} \times t \quad (2)$$

where Q is the heat produced, V is the applied potential, R is the resistance of the electrode, and t is the working time. The higher

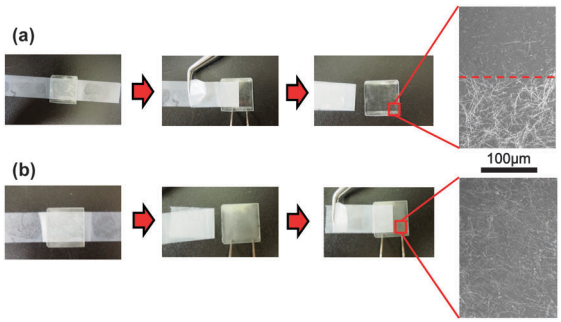

Fig. 4 Peeling off test for (a) the AgNW electrode without binder and (b) the AgNW–PI hybrid electrode by 3 M scotch tape. The SEM images used to observe the morphology of the electrodes after the peeling off test.

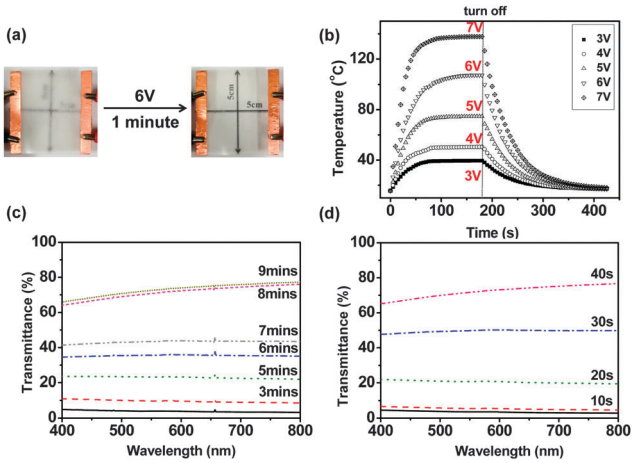

Fig. 5 (a) The defogging device fabricated from AgNW–PI hybrids was put in a refrigerator and then subjected to an applied potential of 6 V, the water on the surface was removed after only one minute. (b) The temperature plotted against time at various applied potentials. (c) UV-vis spectra for the defogging device without any applied potential. (d) UV-vis spectra for the defogging device with an applied potential of 6 V.

the applied potential on the device, the higher a temperature could be reached (Fig. 5b). As the applied potential was increased to 7 V, a temperature higher than 130 °C could be obtained. Therefore, the thermal stability of both the substrates and binders should be good enough to withstand such high temperatures, and that will not be an issue when using PI as substrates and binders. The defogging behavior of the device without any applied potential took about 10 minutes to recover the original visibility, as shown in Fig. 5c. When a potential of 6 V was applied (Fig. 5d), by measuring the recovery of transmittance from the UV-vis spectra, we determined that the condensed water on the device could be removed within only one minute. The cycling heating performance measurement of the AgNW–PI defogging device for evaluating long-term stability was also conducted and is shown in Fig. S1 (ESI†). For the application of windshields in automobiles, the occurrence probability of an accident may be reduced by removing condensed water on the windshield more effectively. Moreover, this approach can also replace the traditional defogger on a vehicle's rear windshield, which consists of a series of parallel linear resistive conductors.

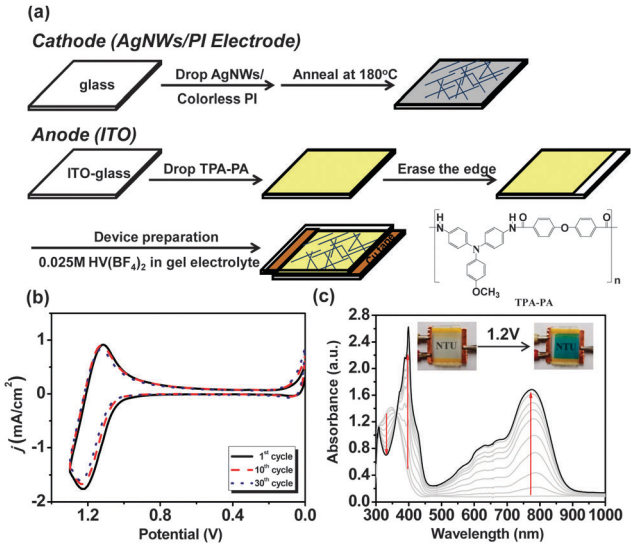

Fig. 6 (a) The scheme of the procedure for the electrochromic device based on the AgNW–PI hybrid electrode. (b) Cyclic voltammetric diagrams of the ECD based on the AgNW–PI electrode for 30 cycles. (c) The electrochromic behavior of the ECD by using the AgNW–PI hybrid electrode and ITO coated glass as the cathode and anode, respectively.

Without the parallel linear resistive conductors on the back glass, it would be more pleasing to the eyes.

3.4 Properties of the electrochromic device based on the AgNW–PI electrode

The AgNW–PI hybrid electrodes were also applied to electrochromic devices (ECD). The scheme of the procedure for the electrochromic device using an AgNW–PI hybrid electrode is depicted in Fig. 6a, and the electrochemical behavior for the ECD of TPA–PA[43] was investigated by cyclic voltammetry (CV). A polyamide film was cast on an indium tin oxide (ITO)-coated glass substrate as the working electrode. The AgNW–PI electrode was used as the cathode. The oxidation and reduction cycles of the film samples were measured in the form of a device with gel electrolytes, using PMMA as the stiffener, propylene carbonate as the solvent, $LiBF_4$ as the electrolyte, and $HV(BF_4)_2$ as the counter electrode species or ion storage layer. A typical CV diagram for the ECD based on AgNW–PI electrodes is illustrated in Fig. 6b. The CV measurements reveal reversible oxidation coupled with an $E_{1/2}$ value of 1.09 V and good electrochemical stability. Spectroelectrochemical experiments were used to evaluate the optical properties of the electrochromic behavior. The device was placed in the optical path of the sample light beam in a UV-vis-NIR spectrophotometer, which allowed us to acquire electronic absorption spectra under a potential control. A typical spectroelectrochemical spectrum of the device is shown in Fig. 6c. It exhibits strong absorption at 345 nm, characteristic for the TPA moiety in the neutral form (0.0 V), implying a high optical transparency and almost colorless behavior in the visible region. Upon oxidation (applied voltage was changed from 0.0 to 1.2 V), the intensity of the absorption peak at 345 nm gradually decreased, while new peaks at 389 nm and 787 nm simultaneously increased

in intensity due to the formation of a monocation radical of the TPA unit. In addition, other new peaks at 399 nm and 605 nm also increased in intensity due to the formation of a monocation radical of the viologen moiety by gaining one electron. Combining these two electrochromic materials, the color switched from an almost colorless neutral state (0.00 V) to blue/green (1.2 V) with a very high contrast of optical transmittance at 787 nm.

5. Conclusions

In conclusion, a facile solution casting method without transfer of AgNWs has been demonstrated as an effective approach to prepare transparent electrodes in this study. Introducing colorless PI into the AgNWs as a binder not only prevents the peeling off from substrates due to the weak adhesion between AgNWs and substrates, but also enhances the dispersion of the nanowires. The resulting flexible AgNW–PI hybrid electrodes exhibited high transparency and high electrical conductivity with a FoM value up to 160. In addition, the excellent heat-resistance properties and thermal stability of these AgNW–PI hybrid electrodes afford the potential to operate under high temperatures in the working environment and also serve as the electrodes for wearable devices.

Notes and references

1 S. Iijima, *Nature*, 1991, **354**, 56–58.
2 K. S. Novoselov, A. K. Geim, S. V. Morozov, D. Jiang, Y. Zhang, S. V. Dubonos, I. V. Grigorieva and A. A. Firsov, *Science*, 2004, **306**, 666–669.
3 J.-Y. Lee, S. T. Connor, Y. Cui and P. Peumans, *Nano Lett.*, 2008, **8**, 689–692.
4 A. R. Rathmell and B. J. Wiley, *Adv. Mater.*, 2011, **23**, 4798–4803.
5 J. Li, L. Hu, L. Wang, Y. Zhou, G. Grüner and T. J. Marks, *Nano Lett.*, 2006, **6**, 2472–2477.
6 (*a*) E. Braun, Y. Eichen, U. Sivan and G. B. Yoseph, *Nature*, 1998, **391**, 775–778; (*b*) L. Huang, H. Wang, Z. Wang, A. Mitra, K. N. Bozhilov and Y. Yan, *Adv. Mater.*, 2002, **14**, 61–64; (*c*) C. J. Murphy and N. R. Jana, *Adv. Mater.*, 2002, **14**, 80–82.
7 Y. Sun, Y. Yin, B. T. Mayers, T. Herricks and Y. Xia, *Chem. Mater.*, 2002, **14**, 4736–4745.
8 J. Jiu, M. Nogi, T. Sugahara, T. Tokuno, T. Araki, N. Komoda, K. Suganuma, H. Uchidab and K. Shinozaki, *J. Mater. Chem.*, 2012, **22**, 23561–23567.
9 T. Tokuno, M. Nogi, J. Jiu, T. Sugahara and K. Suganuma, *Langmuir*, 2012, **28**, 9298–9302.
10 C. Gong, J. Liang, W. Hu, X. Niu, S. Ma, H. T. Hahn and Q. Pei, *Adv. Mater.*, 2013, **25**, 4186–4191.
11 L. Hu, H. S. Kim, J.-Y. Lee, P. Peumans and Y. Cui, *ACS Nano*, 2010, **4**, 2955–2963.
12 W. Gaynor, G. F. Burkhard, M. D. McGehee and P. Peumans, *Adv. Mater.*, 2011, **23**, 2905–2910.
13 P. Lee, J. Lee, H. Leem, J. Yeo, S. Hong, K. H. Nam, D. Lee, S. S. Lee and S. H. Ko, *Adv. Mater.*, 2012, **24**, 3326–3332.
14 A. R. Madaria, A. Kumar, F. N. Ishikawa and C. Zhou, *Nano Res.*, 2010, **3**, 564–573.
15 S. Zhu, Y. Gao, B. Hu, J. Li, J. Su and Z. Su, *Nanotechnology*, 2013, **24**, 335202.
16 T. Kim, A. Canlier, G. H. Kim, J. Choi, M. Park and S. M. Han, *ACS Appl. Mater. Interfaces*, 2013, **5**, 788–794.
17 M. S. Miller, J. C. O'Kane, A. Niec, R. S. Carmichael and T. B. Carmichael, *ACS Appl. Mater. Interfaces*, 2013, **5**, 10165–10172.
18 C.-H. Liu and X. Yu, *Nanoscale Res. Lett.*, 2011, **6**, 75–82.
19 Y.-C. Lu and K.-S. Chou, *Nanotechnology*, 2010, **21**, 215707.
20 S. Nam, M. Song, D.-H. Kim, B. Cho, H. M. Lee, J.-D. Kwon, S.-G. Park, K.-S. Nam, Y. Jeong, S.-H. Kwon, Y. C. Park, S.-H. Jin, J.-W. Kang, S. Jo and C. S. Kim, *Sci. Rep.*, 2013, **4**, 4788.
21 J. Liang, L. Li, X. Niu, Z. Yu and Q. Pei, *Nat. Photonics*, 2013, **7**, 817–824.
22 Z. Yu, L. Li, Q. Zhang, W. Hu and Q. Pei, *Adv. Mater.*, 2011, **23**, 4453–4457.
23 L. Yang, T. Zhang, H. Zhou, S. C. Price, B. J. Wiley and W. You, *ACS Appl. Mater. Interfaces*, 2011, **3**, 4075–4084.
24 C.-C. Chen, L. Dou, R. Zhu, C.-H. Chung, T.-B. Song, Y. B. Zheng, S. Hawks, G. Li, P. S. Weiss and Y. Yang, *ACS Nano*, 2012, **6**, 7185–7190.
25 K.-H. Choi, J. Kim, Y.-J. Noh, S.-I. Na and H.-K. Kim, *Sol. Energy Mater. Sol. Cells*, 2013, **110**, 147–153.
26 J.-W. Lim, D.-Y. Cho, E. Eun, S.-H. Choa, S.-I. Na, J. Kim and H.-K. Kim, *Sol. Energy Mater. Sol. Cells*, 2012, **105**, 69–76.
27 M. Song, D. S. You, K. Lim, S. Park, S. Jung, C. S. Kim, D.-H. Kim, D.-G. Kim, J.-K. Kim, J. Park, Y.-C. Kang, J. Heo, S.-H. Jin, J. H. Park and J.-W. Kang, *Adv. Funct. Mater.*, 2013, **23**, 4177–4184.
28 J. Lee, P. Lee, H. B. Lee, S. Hong, I. Lee, J. Yeo, S. S. Lee, T. S. Kim, D. Lee and S. H. Ko, *Adv. Funct. Mater.*, 2013, **23**, 4171–4176.
29 C. Celle, C. Mayousse, E. Moreau, H. Basti, A. Carella and J. P. Simonato, *Nano Res.*, 2012, **5**, 427–433.
30 T. Y. Kim, Y. W. Kim, H. S. Lee, H. Kim, W. S. Yang and K. S. Suh, *Adv. Funct. Mater.*, 2013, **23**, 1250–1255.
31 S. Sorel, D. Bellet and J. N Coleman, *ACS Nano*, 2014, **8**, 4805–4814.
32 S. Ji, W. He, K. Wang, Y. Ran and C. Ye, *Small*, 2014, **10**(23), 4951–4960.
33 J. Li, J. Liang, X. Jian, W. Hu, J. Li and Q. Pei, *Macromol. Mater. Eng.*, 2014, **299**, 1403–1409.
34 L. Li, Z. Yu, W. Hu, C. H. Chang, Q. Chen and Q. Pei, *Adv. Mater.*, 2011, **23**, 5563–5567.
35 S. Coskun, E. S. Ates and H. E. Unalan, *Nanotechnology*, 2013, **24**, 125202.
36 X.-Y. Zeng, Q.-K. Zhang, R.-M. Yu and C.-Z. Lu, *Adv. Mater.*, 2010, **22**, 4484–4488.
37 H.-J. Yen, C.-J. Chen and G.-S. Liou, *Adv. Funct. Mater.*, 2013, **23**, 5307–5316.
38 C. Yan, W. Kang, J. Wang, M. Cui, X. Wang, C. Y. Foo, K. J. Chee and P. S. Lee, *ACS Nano*, 2014, **8**, 316–322.
39 C.-J. Chen, Y.-C. Hu and G.-S. Liou, *Chem. Commun.*, 2013, **49**, 2536–2538.
40 M. Hu, J. Gao, Y. Dong, K. Li, G. Shan, S. Yang and R. K.-Y. Li, *Langmuir*, 2012, **28**, 7101–7106.

41 D. Y. Choi, H. W. Kang, H. J. Sung and S. S. Kim, *Nanoscale*, 2013, **5**, 977–983.
42 D. S. Ghosh, T. L. Chen, V. Mkhitaryan and V. Pruneri, *ACS Appl. Mater. Interfaces*, 2014, **6**, 20943–20948.
43 C.-W. Chang, G.-S. Liou and S.-H. Hsiao, *J. Mater. Chem.*, 2007, **17**, 1007–1015.
44 M. Hasegawa, D. Hirano, M. Fujii, M. Haga, E. Takezawa, S. Yamaguchi, A. Ishikawa and T. Kagayama, *J. Polym. Sci., Part A: Polym. Chem.*, 2013, **51**, 575–592.
45 T. Ogura and M. Ueda, *Macromolecules*, 2007, **40**, 3527–3529.
46 J.-Y. Lee, S. T. Connor, Y. Cui and P. Peumans, *Nano Lett.*, 2010, **10**, 1276–1279.
47 G. Haacke, *J. Appl. Phys.*, 1976, **47**, 4086–4089.
48 M. Dressel and G. Grüner, *Electrodynamics of solids: Optical, Properties of Electrons in Matter*, Cambridge University Press, Cambridge, 2002, pp. 265–275.
49 S. De, T. M. Higgins, P. E Lyons, E. M. Doherty, P. N. Nirmalraj, W. J. Blau, J. J. Boland and J. N Coleman, *ACS Nano*, 2009, **3**, 1767–1774.
50 S. Sorel, P. E Lyons, S. De, J. C Dickerson and J. N Coleman, *Nanotechnology*, 2012, **23**, 185201.